Multipole moments of ^{166}Er, ^{168}Er, ^{174}Yb, and ^{176}Yb from 65 MeV polarized proton inelastic scattering and density dependence of the effective interaction

T. Ichihara, H. Sakaguchi, M. Nakamura, T. Noro,* F. Ohtani,† H. Sakamoto,‡ H. Ogawa, M. Yosoi, M. Ieiri, N. Isshiki, and S. Kobayashi
Department of Physics, Kyoto University, Kyoto 606, Japan
(Received 24 October 1983)

Differential cross sections and analyzing powers of polarized proton elastic and inelastic scattering from ^{166}Er, ^{168}Er, ^{174}Yb, and ^{176}Yb have been measured at 65 MeV. Analysis for $J^\pi=0^+-6^+$ members of the ground state rotational band has been performed using coupled-channel calculations for scattering from deformed optical potentials. Excellent fits have been obtained for both cross sections and analyzing powers for 0^+, 2^+, and 4^+ states and fairly good fits for the 6^+ state. In the coupled-channel calculations, the multipole moments of each part of the deformed optical potentials were set to be equal. The quadrupole moments of the deformed optical potentials for these nuclei were found to be 4—6% larger than those of charge densities obtained by electron scattering and Coulomb excitation. A folding model calculation shows that the main part of this difference is attributed to the density dependence of the effective interaction. Mass number dependence of the phenomenological range of the effective interaction can be also reproduced from the folding calculation using the density-dependent effective interaction.

I. INTRODUCTION

Recent progress in nuclear matter theory has stimulated the study of nuclear reactions in terms of realistic nucleon-nucleon interactions. In particular, the microscopic optical potential has enabled us to describe elastic scattering of protons[1,2] from spherical nuclei globally. For the inelastic scattering from low-lying collective states, it has just started to explain the scattering from the microscopic standpoint. Experimentally, the progress in high quality beams and high resolution spectrographs has made it possible recently to measure the low-lying inelastic scattering of hadrons and electrons from deformed nuclei in the $152 \leq A \leq 190$ region, where the theoretical treatment is simple and clear. The recent central concern in inelastic scattering from low-lying states in deformed nuclei lies in interpreting the difference between multipole moments observed by various probes. One of the keys to solving this problem is Satchler's theorem,[3] which states that the multipole moments of the folded potential are equal to those of underlying matter distribution if the effective interaction is local and density independent. However much evidence has been reported[4–11] that the effective interaction is density dependent; careful consideration should be given in the application of Satchler's theorem.

Up to now, many experimental efforts[12–17] have been devoted to resolve such problems, but some of their results are complicated. King *et al.*[12] have shown using 35 MeV protons that the quadrupole moments of the deformed optical potentials (DOP) are systematically ($\leq 6\%$) smaller than those of the charge densities for ^{154}Sm, ^{176}Yb, ^{232}Th, and ^{238}U. An experiment using 800 MeV protons was performed at the Los Alamos Meson Physics Facility (LAMPF) by Barlett *et al.*,[13] and their analysis has shown that the multipole moments of the imaginary part of the DOP are almost equal to those of the charge densities for ^{154}Sm and ^{176}Yb. On the other hand, the quadrupole moments of the DOP obtained by inelastic scattering of the polarized proton at 134 MeV on ^{154}Sm and ^{166}Er by Ronningen *et al.*[14] are about 4—11% larger than the charge quadrupole moments.

We have measured the cross sections and analyzing powers of polarized proton elastic and inelastic scattering from ^{166}Er, ^{168}Er, ^{174}Yb, and ^{176}Yb at 65 MeV. The experiment using 65-MeV polarized protons[1,2] has many advantages. First, at this energy the influence of a giant resonance on the excitation of a low-lying collective state is small and the reaction mechanism is relatively simple. Second, the DOP parameters can be determined with less ambiguities using the analyzing power data together with the cross sections, and therefore the multipole moments of the DOP can be determined precisely. Furthermore, in this energy region the real central part of the optical potential is deep, in contrast to the intermediate and high energy region, where the imaginary part of the optical potential plays an important role.

The work presented here is aimed at extracting the multipole moments of the DOP and comparing them with the charge multipole moments, and also interpreting them in terms of the folding model and the properties of the effective interaction in this energy region. In this paper, we describe the experimental method in Sec. II, and the method of the data reduction in Sec. III. The conventional optical model analysis and the coupled channel analysis are presented in Sec. IV. The comparison of the multipole moments of the DOP derived from our experiment with those of the charge densities is presented in Sec. V and also the effect of the density dependence of the effective interaction is discussed through the folding calculations. A summary and some conclusions are given in Sec. VI. The details of the folding calculation are described in Ap-

pendix A, and the range of the effective interaction is investigated in Appendix B.

II. EXPERIMENTAL METHOD

The experiment has been performed using polarized protons from the azimuthally varying field (AVF) cyclotron at the Research Center for Nuclear Physics (RCNP), Osaka University, and the data have been obtained using the high resolution spectrograph RAIDEN.[18] The polarized proton beam from the atomic beam-type polarized ion source[19] (PIS) is injected axially into the cyclotron. The injection system is controlled by a microcomputer system, so that the stable operation of the PIS is achieved. The beam from the cyclotron was momentum analyzed by double analyzing magnets,[20] and deflected again by a cleaning magnet to reduce beam background. The beam spot size on target was about 1.0 mm in diameter.

During the experiment the beam polarization was monitored by a sampling-type beam polarimeter,[21] which was located at the focal point upstream of the cleaning magnet. A stacked polyethylene target was periodically inserted in the beam line for a few seconds with an interval of 10—50 sec. The beam polarization was monitored while the polarimeter target was in the beam line. The measurement with the spectrograph was carried out when the polarimeter target was out of the beam line. The direction of the beam polarization was reversed every 0.5 sec by switching the rf transitions at the PIS.

At the focal plane of the spectrograph, scattered particles were detected by a counter array[22] consisting of a two-dimensional position sensitive proportional counter of 1.5 m length, a dual single wire proportional counter, and a plastic scintillation counter. The horizontal position along the focal plane was measured by the charge division method, and the vertical position was determined by measuring the drift time of the electrons. A pileup rejecter was employed to prevent pileup signals from causing a yield at an unexpected position. An event signal was generated by an energy signal from the plastic scintillator, and when an event occurred, every signal was digitalized by analog-to-digital converters (ADC's) and transmitted into a PDP-11/44 computer through the raw data processor.[23] At the PDP-11/44 computer, all data were recorded on magnetic tape in a list mode.

The targets used were self-supporting enriched metal foils, and their thicknesses and isotopic enrichments are summarized in Table I. The solid angles and angular acceptances were 1.2 msr and $\pm 0.46°$ for measurements at forward angles ($\theta_{lab} \leq 36°$) and 2.3 msr and $\pm 0.71°$ for measurements at backward angles ($\theta_{lab} > 36°$). The absolute scattering angle was determined with the accuracy of 0.05° by searching the scattering angle at which the sign of the analyzing power of the p + ^{208}Pb elastic scattering changes rapidly ($\theta_{lab} = 29.81°$ at $E_p = 65$ MeV). The angular distributions were measured from 11° to 70° in 1.0° steps at forward angles and in 2.0° steps at backward angles. The elastic peak was always kept at the same position on the focal plane counter in the measurements of the angular distributions in order to avoid the systematic errors which might arise from unevenness of the efficiency.

TABLE I. Thicknesses and isotopic enrichments of the targets.

Target	Thickness (mg/cm^2)	Enrichment
^{166}Er	2.0	97.69%
^{168}Er	2.0	96.24%
^{174}Yb	1.0	95.80%
^{176}Yb	1.0	96.68%

The overall energy resolution and beam intensities on target were 20—22 keV FWHM and 20 nA at forward angles, and 24—26 keV FWHM and 40 nA at backward angles. In the measurement of the very forward angles ($\theta_{lab} \leq 15°$), the width of the slits in the beam transport system was adjusted in order to obtain proper counting rate (≤ 800 cps) and a better energy resolution. The well-separated elastic peak from a ^{148}Sm target with 2.0 mg/cm^2 thickness was measured with good statistical accuracy as a reference spectrum in peak fitting.

III. DATA REDUCTION AND RESULT

List mode raw data on magnetic tapes were sorted event by event, and finally the position spectra were constructed employing a particle identification gate. The overall dead time corrections were carried out for the position spectra assuming constant efficiency of the plastic scintillator, and these did not exceed 6%. These counting losses arose mainly from the pileup rejecter and the dead time of counter system and ADC's. Figures 1 and 2 show typical position spectra for ^{166}Er and ^{174}Yb at $\theta_{lab} = 48°$. It is notable that the peak-to-valley ratio between 0^+ and 2^+ states is more than ten. Even at the very forward angle the separation is excellent as shown in Ref. 2.

For the 0^+, 2^+, and 4^+ states of the ground state rotational band of Er isotopes and 0^+ and 2^+ states of Yb isotopes, peak areas were extracted using a peak fitting code assuming that the peak shapes were identical for these states. The peak shape function was extracted from the elastic peak itself except for the tail at the low momentum side, which was taken from the well-separated reference spectrum of ^{148}Sm. The χ^2 values per data point in the peak fitting were 1.0—1.5. The statistical uncertainties of the peak sums were calculated by solving the error matrix (inverse of the matrix of second derivatives of χ^2) in the peak fitting procedures.

The beam polarization was calculated for the spin up and spin down modes independently for every run, and they were nearly equal to 80%. The difference in the beam polarization between the spin up mode and spin down mode was less than 2%.

The experimental cross sections and analyzing powers are plotted in Figs. 3—6. The error bars on experimental data represent only statistical ones.

IV. ANALYSIS

In the analysis of the conventional optical potential and coupled channel calculation, 3% errors were added to the statistical uncertainties in quadrature to include the un-

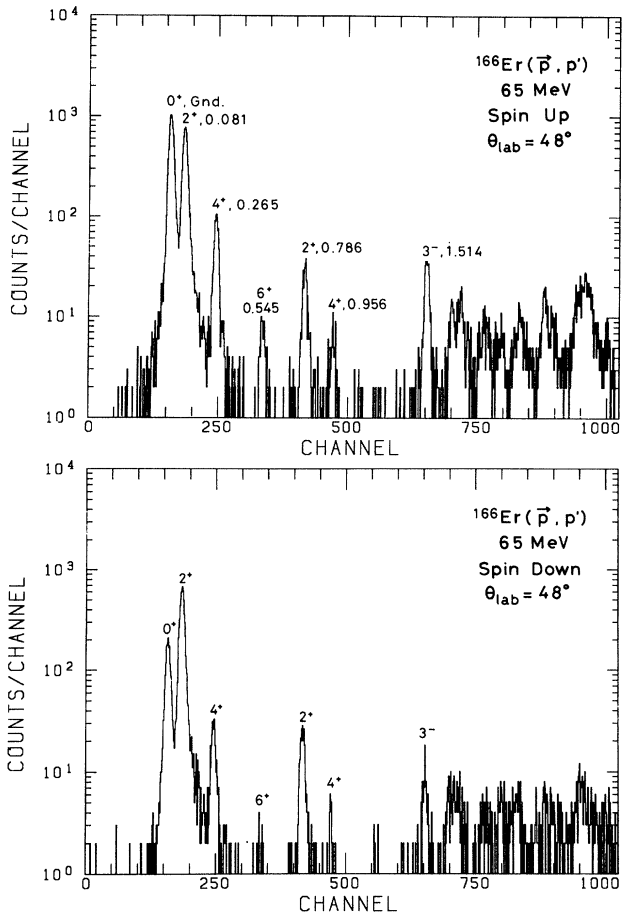

FIG. 1. Typical position spectra of the focal plane counter for the ^{166}Er(p,p') scattering at 65 MeV. Spin up and spin down spectra are shown at θ_{lab}=48°.

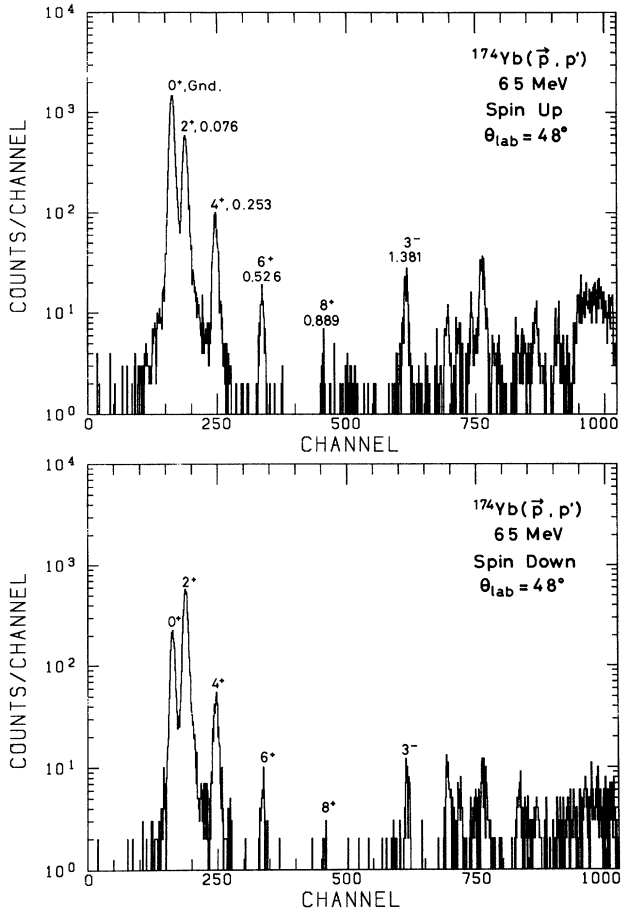

FIG. 2. Same as Fig. 1 except for ^{174}Yb.

known systematic error and to avoid trapping in an unphysical local χ^2 minimum as shown in the following forms:

$$\delta\left[\frac{d\sigma}{d\Omega}\right]=\left[\delta\left[\frac{d\sigma}{d\Omega}\right]_{\text{stat}}^2+\left[\frac{d\sigma}{d\Omega}\right]^2\times 0.03^2\right]^{1/2}, \quad (1)$$

$$\delta Ay=(\delta Ay_{\text{stat}}^2+0.03^2)^{1/2}. \quad (2)$$

A. Optical potential for elastic scattering

Conventional optical potential fitting to the elastic scattering data was performed using the automatic search code MAGALI (Ref. 24) of Raynal. The following optical potential was used:

$$U(r)=V_{\text{Coul}}(r)-V_R f(r;r_R,a_R) -iW_v f(r;r_{wv},a_{wv})+4ia_{ws}W_s\frac{d}{dr}f(r;r_{ws},a_{ws}) +V_{ls}\left[\frac{\hbar}{m_\pi c}\right]^2\frac{1}{r}\frac{d}{dr}f(r;r_{ls},a_{ls})(\vec{\sigma}\cdot\vec{L}), \quad (3)$$

where

$$f(r;r_0,a_0)=\{1+\exp[(r-r_0A^{1/3})/a_0]\}^{-1},$$

$$V_{\text{Coul}}(r)=\begin{cases}\dfrac{Ze^2}{2r_cA^{1/3}}\left[3-\dfrac{r^2}{r_c^2A^{2/3}}\right] & r\le r_cA^{1/3}\\ \dfrac{Ze^2}{r} & r>r_cA^{1/3}.\end{cases}$$

All parameters except for the Coulomb potential were searched. A renormalization of the experimental cross sections was included taking account of the uncertainties of the target thicknesses. The best fit optical potential parameters are shown in Table II. The χ^2 per data point are 0.3—0.5.

B. Coupled channel analysis

Coupled channel analysis[25] has been performed for the $j^\pi=0^+-6^+$ states of the ground state rotational bands using the automatic search code ECIS79 (Ref. 26) of Raynal. It was assumed that these states are members of a $K^\pi=0^+$ rotational band of the axially symmetric rigid rotor. In the coupled channel calculation, the deformed optical potential (DOP) was produced by replacing the radius parameters of each part of the optical potential (3) by

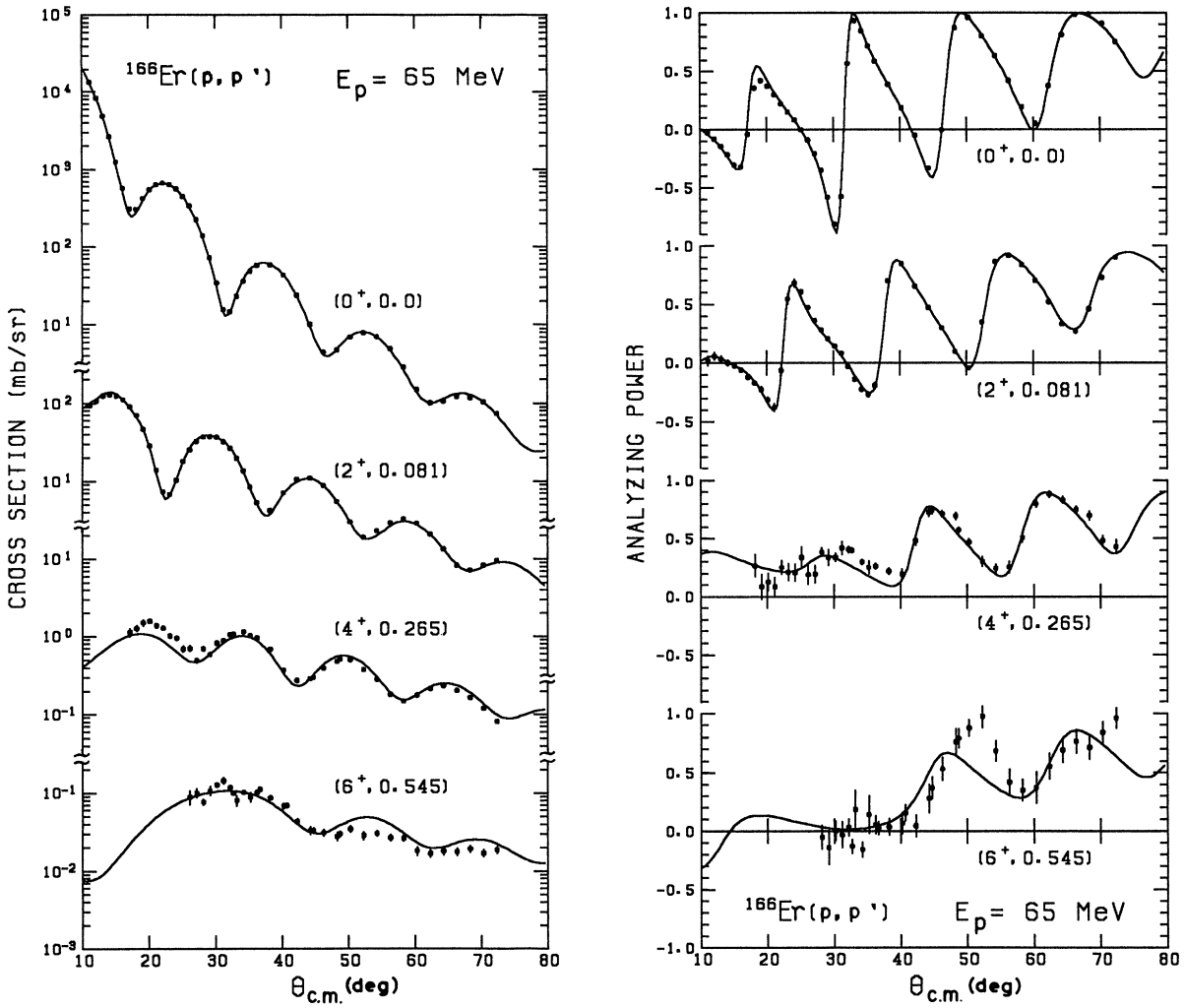

FIG. 3. Measured cross sections and analyzing powers for the ^{166}Er(p,p') scattering at 65 MeV. The error bars on the experimental data represent only statistical ones. The solid curves are results of the coupled-channel calculations with the DOP. The DOP parameters are listed in Tables II and III.

$$r^j(\theta)=r_0^j\left[1.0+\sum_\lambda \beta_\lambda^j Y_{\lambda 0}(\theta)\right], \tag{4}$$

where the suffix j represents each part of the optical potentials; the real central part, the volume imaginary part, and so on. The deformation parameters β_2^j, β_4^j, and β_6^j were used. The DOP was expanded in multipoles up to $\lambda=12$. The deformed full-Thomas term[27] was used for the spin-orbit potential. The Coulomb potential was that of deformed Fermi distribution, the reduced radius r_c and the diffuseness a_c were kept as $r_c=1.11$ fm and $a_c=0.58$ fm. These values were obtained from the electron scattering data and modified in consideration of the finite charge distribution in the projectile proton itself. The influence of the Coulomb distortion due to the deformation still remains beyond the matching radius (20 fm), so we used the Coulomb correction[28] for the distortion beyond the matching radius.

The reduced multipole moments of the DOP are given as follows: (In this paper, we mention this reduced multipole moment simply as the multipole moment.)

$$Q_\lambda=\frac{Ze}{J_v}\int V(r,\theta)Y_{\lambda 0}(\theta)r^{\lambda+2}dr\,d\Omega\,, \tag{5}$$

where J_v represents the volume integral of the DOP as

$$J_v=\int V(r,\theta)r^2dr\,d\Omega\,. \tag{6}$$

Generally, in the coupled channel calculations of the deformed nuclei, there is a problem of how to relate the deformation parameters of each part of the optical potential.[10,29,30] According to Satchler's theorem,[3] a reasonable constraint on each deformation parameter is the requirement that they produce equal multipole moments of each part of the optical potentials,[29,30] although the same defor-

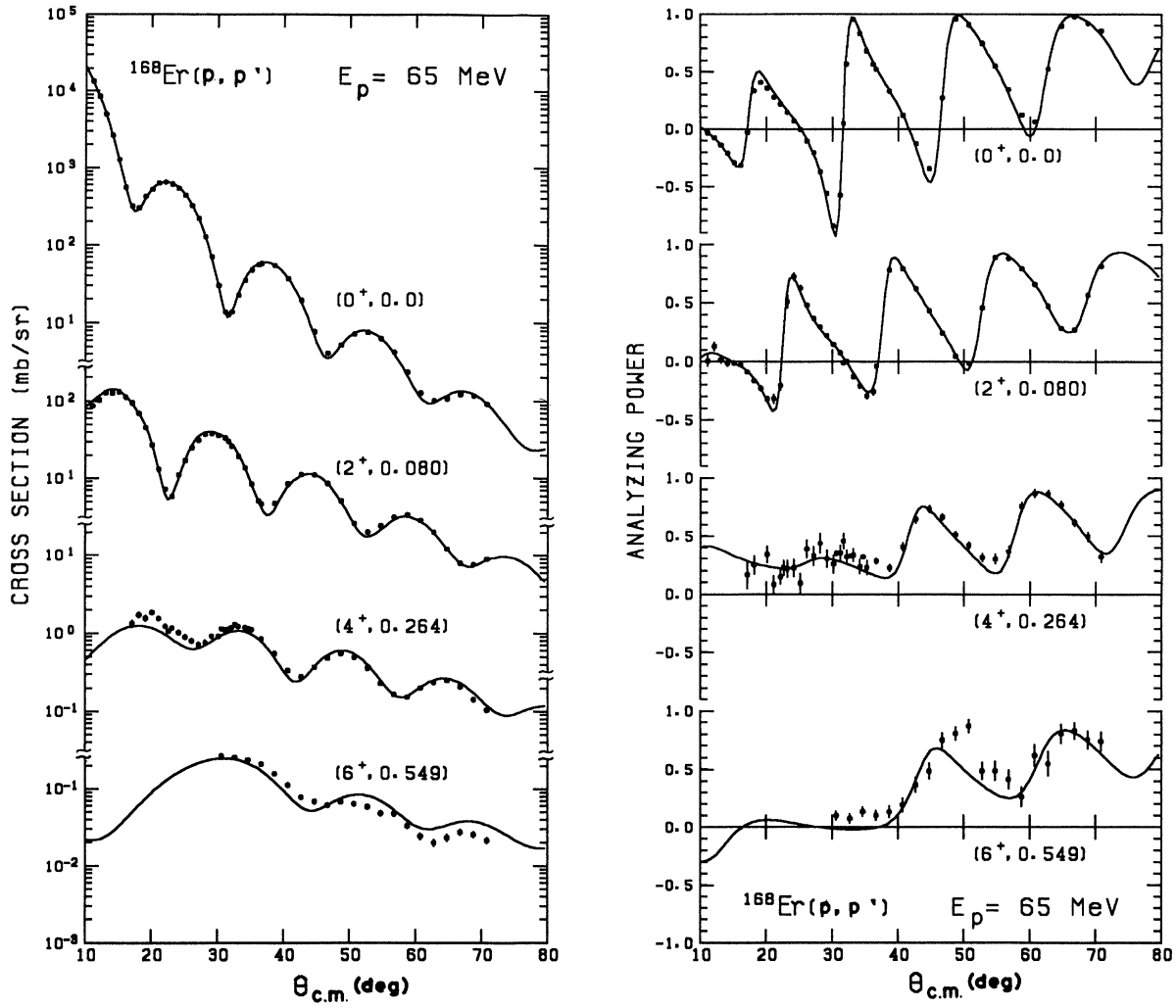

FIG. 4. Same as Fig. 3 except for ^{168}Er.

mation parameters, or sometimes deformation length (βR) scaling, have been used so far.

Therefore we modified the ECIS79 by adding some subroutines to perform the following procedures. In each calculation, the multipole moments of the real central potential were calculated first, and then the deformation parameters of the other parts of the optical potential were calculated so as to reproduce the multipole moments of the real central potential by expanding them in the first order and using Newton's method. For the differential type of potential, the surface imaginary part and spin-orbit part, the multipole moments of the deformed Fermi form factors were calculated, not the differential ones. The Coulomb deformation parameters were set to reproduce the charge multipole moments obtained by electron scattering and Coulomb excitation.

Using this modified ECIS79, every part of the DOP parameters and multipole moments (i.e., deformation parameters) were searched with various combinations of the search parameters. Usually 4—7 parameters were searched at the same time. The calculation where each deformation parameter was set to be equal and the Coulomb correction was not employed increased χ^2 about 10—40 %, and also increased the quadrupole moment of the DOP about 0—2 %. During the search of the coupled channel calculations, renormalization factors for the experimental cross sections were also adjusted.

Solid curves in Figs. 3—6 show the best fit calculations to the data, and the DOP parameters are listed in Tables II and III. As shown in the figures excellent fits have been obtained for 0^+, 2^+, and 4^+ states and fairly good fits for 6^+ states.

In order to investigate the sensitivity of the data to the multipole moments, χ^2 values for each state were evaluated with a little variation of each multipole moment except for the Coulomb potential. Typical results for ^{166}Er are shown in Fig. 7. In this paper, the uncertainties in the multipole moments have been defined by the values where the χ^2 value increases 10% from the minimum one. These uncertainties are not statistical, but represent the

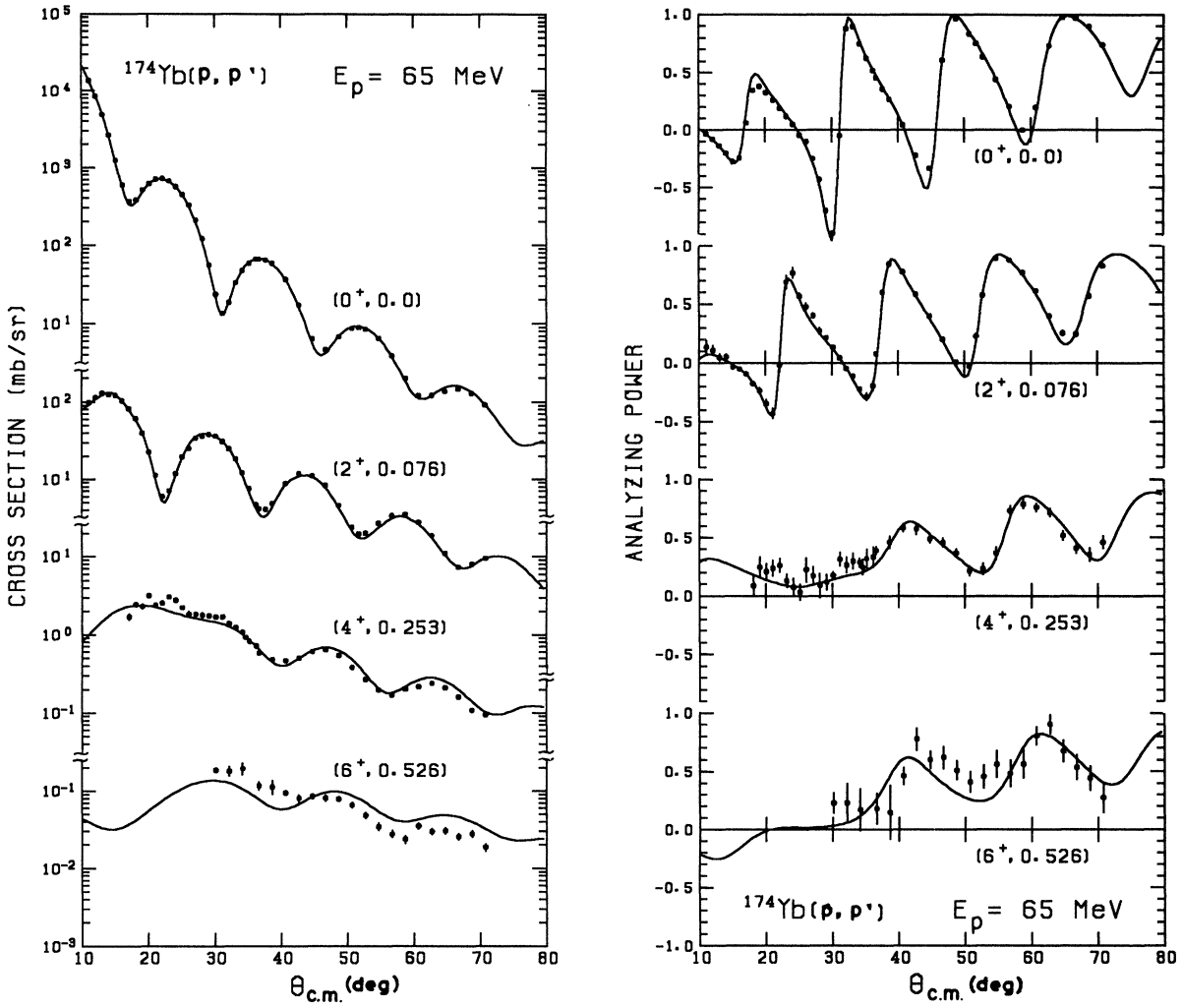

FIG. 5. Same as Fig. 3 except for ^{174}Yb.

sensitivity of the experimental data to the multipole moments.

V. DISCUSSION

A. Optical potential

The differences between the spherical optical potential (SOP) which reproduces only elastic scattering and the DOP derived from the coupled channel calculations have been discussed in detail in our previous paper,[2] so we mention these briefly.

The volume integrals of real central potential per nucleon of the DOP are about 14—17 MeV fm^3 larger than those of the SOP as listed in Table II. The effect of the collective excitations on the real central potential is repulsive. This phenomenon was also observed in (α,α') reactions,[16] in (d,d') reactions,[17] and in (p,p') reactions.[2]

Another difference between the SOP and DOP is in the shapes of the imaginary parts. In the SOP, the surface region of the imaginary part is deep, in contrast with the spherical nuclei. This is because in the SOP the decrease in the flux due to the collective excitation is taken into account by the imaginary potential whereas in the DOP it is treated explicitly.

With regard to the spin-orbit potential, volume integrals of spin-orbit potentials of the SOP are 20—30% smaller than those of neighboring spherical nuclei, but those of the DOP are very similar to the spherical nuclei as discussed in the previous paper.[2]

B. Multipole moments

It is not reasonable to compare the deformation parameters directly with those obtained by the other experiments, since they depend strongly on the geometry parameters of the optical potential. Therefore, we have compared the multipole moments of the DOP as proposed by Mackintosh.[31] Table IV summarizes the multipole moments of the DOP derived from the present experiment and the other experiments.[12–16,33–40] The multipole moments of the DOP are also shown in Fig. 8, indicated by closed circles, and charge multipole moments are shown as open circles together with the results of the folding cal-

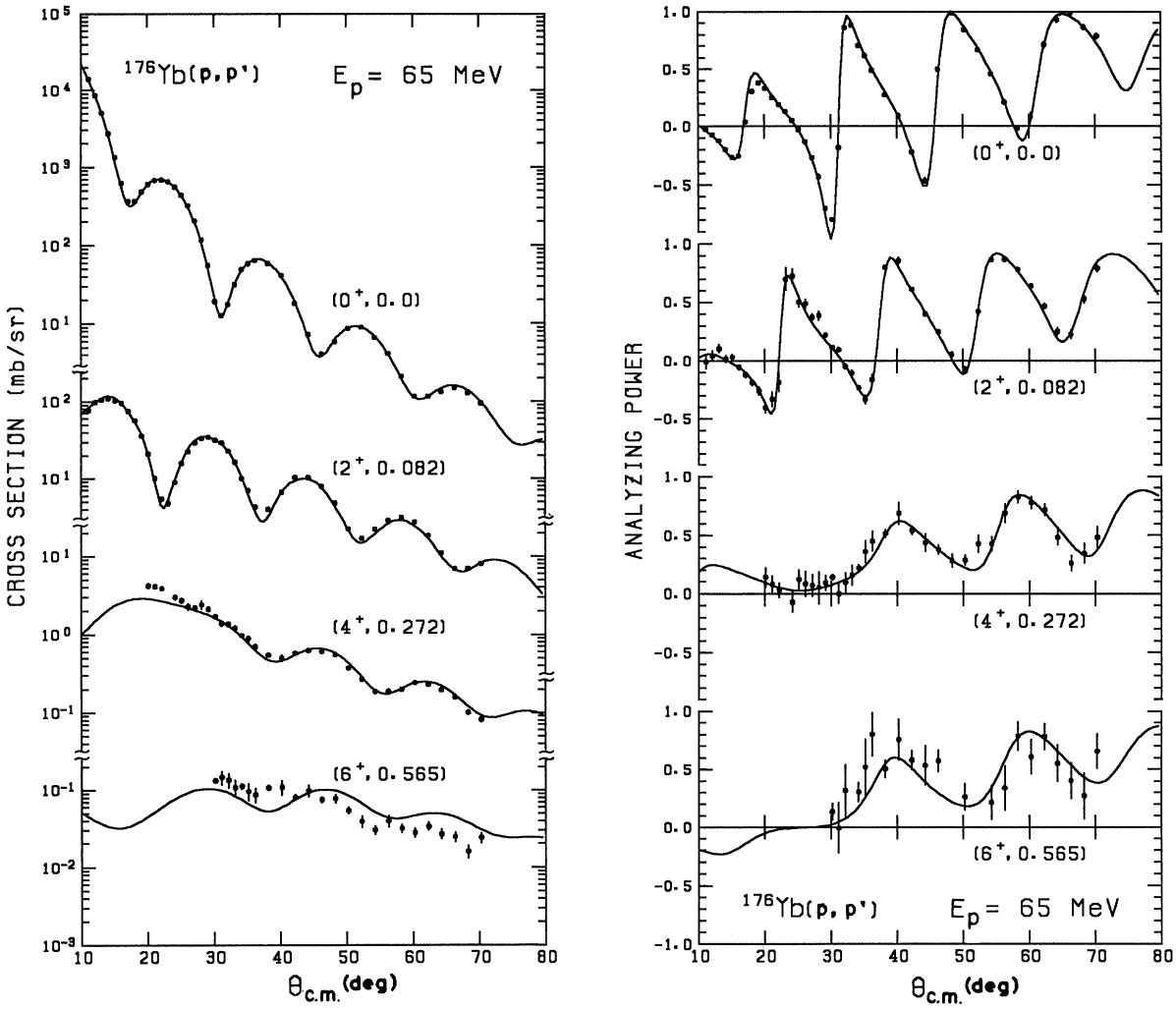

FIG. 6. Same as Fig. 3 except for ^{176}Yb.

culation discussed later. The charge quadrupole moments plotted in Fig. 8 are mean values between the electron scattering[32–34] data and Coulomb excitation data.[35–40] Since the higher charge multipole moments cannot be determined precisely by the experiment of Coulomb excitation, these were taken from the electron scattering data.[33,34]

As shown in the figure, first we notice that the trends of the multipole moments of the DOP and the charge multipole moments agree fairly well. However, it is remarkably observed that the quadrupole moments of our DOP are 4–6 % larger than those of the charge densities for all the measured nuclei. Taking Satchler's theorem into consideration, these differences can be explained in two ways.

(i) The density dependence of the effective interaction causes the quadrupole moments of the DOP to be different from those of underlying matter distributions.

(ii) The quadrupole moments of the proton and neutron distributions are different.

The proton inelastic scattering from ^{154}Sm and ^{176}Yb at 800 MeV (Ref. 13) suggested that the multipole moments of proton and neutron distributions are almost equal. Therefore in order to investigate the effect as listed (i), the folding calculations using the density dependent effective interaction have been carried out.

C. Multipole moments of the folded potential

The details of the folding calculation are described in Appendix A. The density dependent (DD) effective interaction used is the product of the DD function and M3Y effective interaction.[41–43] A δ-function exchange pseudopotential was employed according to Satchler and Love.[44] Two kinds of the DD function were used. The first one is parametrized so as to reproduce the results of the Brueckner-Hartree-Fock (BHF) calculation for nuclear matter by Jeukenne, Lejeune, and Mahaux (JLM).[9] The second one is conventional Green's density dependence as $(1.0–2.0\rho^{2/3})$. Figure 9 shows the shape of these DD functions. Both are normalized at one-third of the normal

TABLE II. Best fit optical potential parameters of the SOP and DOP.

Nucleus	V_R	r_R	a_R	W_v	r_{wv}	a_{wv}	W_s	r_{ws}	a_{ws}	V_{ls}	r_{ls}	a_{ls}	χ^2/N[a]	Renorm	$-J_v$[d]
^{166}Er[b]	36.776	1.226	0.7439	9.211	0.7778	0.3976	8.288	1.178	0.8734	4.914	1.118	0.6906	0.35	1.063	318.0
^{168}Er[b]	36.188	1.226	0.7383	9.757	0.7731	0.3976	8.102	1.178	0.8734	4.853	1.118	0.6906	0.34	1.053	312.5
^{174}Yb[b]	35.259	1.245	0.7200	10.444	0.7898	0.4477	8.463	1.191	0.8205	4.729	1.146	0.6602	0.34	1.130	315.4
^{176}Yb[b]	34.486	1.244	0.7222	9.903	0.8082	0.5255	8.196	1.186	0.8414	4.604	1.145	0.6543	0.51	0.958	307.6
^{166}Er[c]	38.381	1.222	0.7342	7.317	1.421	0.5868	2.323	1.209	0.3793	5.701	1.154	0.6437	0.77	1.049	333.5
^{168}Er[c]	37.578	1.224	0.7211	8.220	1.412	0.5540	1.771	1.202	0.2757	5.670	1.162	0.6307	0.65	0.999	327.1
^{174}Yb[c]	38.572	1.218	0.7312	8.193	1.405	0.5701	1.628	1.225	0.3605	5.721	1.158	0.6605	0.70	1.159	330.9
^{176}Yb[c]	38.452	1.212	0.7306	8.333	1.408	0.5581	1.075	1.184	0.4863	5.642	1.135	0.6607	0.64	0.958	324.9

[a]χ^2 per data point for elastic scattering.

[b]These parameters (SOP) resulted from best-fit searches in conventional optical model analysis for elastic scattering only. The Coulomb potential is that of square well distributions at $r_c = 1.25$ fm.

[c]These parameters (DOP) resulted from best-fit searches in coupled-channel calculations for the members of $J^\pi = 0^+$, 2^+, 4^+, and 6^+ states together with Table III. In the coupled-channel calculation, multipole moments of each form factor of the optical potential were set to be equal except for the Coulomb potential. The Coulomb potential is that of deformed Fermi distribution as $r_c = 1.11$ fm and $a_c = 0.58$ fm and its multipole moments are set to be equal to charge multipole moments.

[d]Volume integrals per nucleon for real central part in MeV fm^3.

TABLE III. Deformation parameters of best fit DOP. (Multipole moments of each form factor of the DOP are equal except for the Coulomb potential. Note that there are only three free parameters for each nucleus in regard to deformation.)

Nucleus	β_2^R	β_4^R	β_6^R	β_2^{wv}	β_4^{wv}	β_6^{wv}	β_2^{ws}	β_4^{ws}	β_6^{ws}	β_2^{ls}	β_4^{ls}	β_6^{ls}	β_2^c	β_4^c	β_6^c	$\chi^2/N(2^+)$	$\chi^2/N(4^+)$	$\chi^2/N(6^+)$
^{166}Er	0.2820	−0.0008	−0.0108	0.2231	−0.0008	−0.0069	0.3041	0.0034	−0.0200	0.3162	+0.0009	−0.0162	0.3258	+0.0148	−0.0126	1.00	5.61	5.21
^{168}Er	0.2873	−0.0088	−0.0183	0.2305	−0.0066	−0.0123	0.3162	−0.0029	−0.0393	0.3198	−0.0083	−0.0270	0.3313	−0.0117	−0.0338	1.22	5.11	10.90
^{174}Yb	0.2797	−0.0351	−0.0119	0.2231	−0.0250	−0.0082	0.2958	−0.0401	−0.0220	0.3131	−0.0423	−0.0178	0.3142	+0.0095	−0.0472	1.36	4.93	11.26
^{176}Yb	0.2714	−0.0478	−0.0090	0.2137	−0.0333	−0.0062	0.2985	−0.0588	−0.0168	0.3104	−0.0604	−0.0141	0.3133	−0.0538	−0.0063	1.43	2.38	6.32

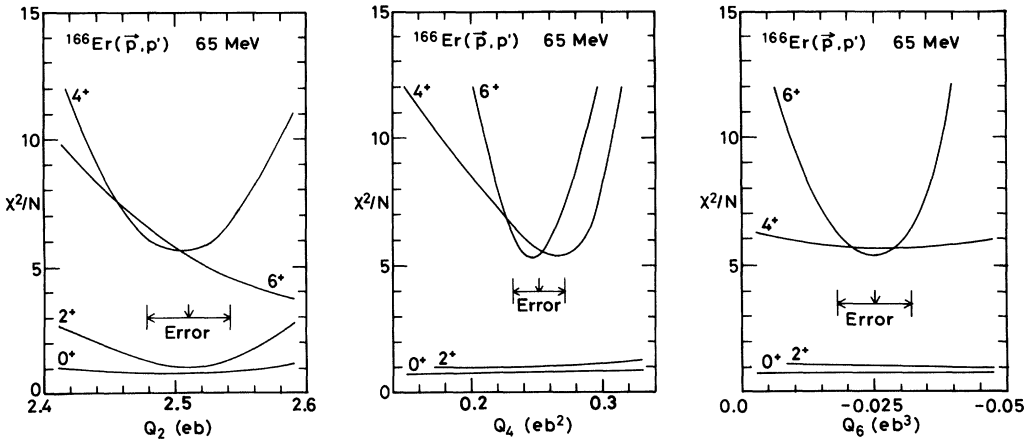

FIG. 7. χ^2 per data point for each state are plotted as a function of each multipole moment. Best fit value and its error (see text) are also drawn as arrows.

TABLE IV. Multipole moments of the DOP and charge densities.

Nucleus	Reaction		Q_2 (e b)	Q_4 (e b^2)	Q_6 (e b^3)	References
^{166}Er	(p,p')	65 MeV	2.511±0.032	0.252 ±0.020	−0.025 ±0.007	This work
	(e,e')	50–320 MeV	2.41	0.294	0.0101	C. W. Creswell (Ref. 33)
	(α,α')	Coulomb excitation	2.378±0.011	0.32 ±0.16		I. Y. Lee *et al.* (Ref. 37)
	(α,α')	Coulomb excitation	2.432±0.005	0.242 ±0.072		H. Fisher *et al.* (Ref. 38)
	(α,α')	Coulomb excitation	2.419±0.009	$0.22^{+0.11}_{-0.16}$		H. J. Wollersheim *et al.* (Ref. 39)
	(α,α')	Coulomb excitation	2.40 ±0.02	$0.06^{+0.12}_{-0.18}$		K. A. Erb *et al.* (Ref. 40)
	(p,p')	134 MeV	2.50 ±0.08	0.32 ±0.06	0.01 ±0.03	R. M. Ronningen *et al.* (Ref. 14)
	(α,α')	50 MeV	2.684	0.275	−0.100	D. L. Hendrie *et al.* (Ref. 16)
	DDHF	p	2.45	0.28		Negele and Rinker (Ref. 49)
		n	2.42	0.32		
^{168}Er	(p,p')	65 MeV	2.564±0.038	0.198 ±0.031	−0.078 ±0.012	This work
	(α,α')	Coulomb excitation	2.43 ±0.02	$0.11^{+0.12}_{-0.18}$		I. Y. Lee *et al.* (Ref. 37)
	(α,α')	Coulomb excitation	2.40 ±0.02	$0.20^{+0.12}_{-0.18}$		K. A. Erb *et al.* (Ref. 40)
^{174}Yb	(p,p')	65 MeV	2.547±0.039	0.025 ±0.031	−0.099 ±0.029	This work
	(e,e')[a]	95–325 MeV	2.28	0.102	−0.060	T. Sasanuma (Ref. 34)
	(α,α')	Coulomb excitation	2.439±0.012	$0.21^{+0.14}_{-0.18}$		H. J. Wollersheim *et al.* (Ref. 35)
	(α,α')	Coulomb excitation	2.433±0.012	0.23 ±0.17		J. S. Greenberg *et al.* (Ref. 36)
	(α,α')	50 MeV	2.750	0.275	−0.088	D. L. Hendrie *et al.* (Ref. 16)
^{176}Yb	(p,p')	65 MeV	2.436±0.032	−0.071 ±0.020	−0.104 ±0.007	This work
	(e,e')	50–320 MeV	2.30	−0.0128	−0.054	C. W. Creswell (Ref. 33)
	(α,α')	Coulomb excitation	2.325±0.019	$0.28^{+0.11}_{-0.20}$		H. J. Wollersheim *et al.* (Ref. 35)
	(p,p')	35 MeV	2.29 ±0.05	−0.09 ±0.03		C. H. King *et al.* (Ref. 12)
	(p,p')[b]	800 MeV	2.31	0.036	−0.048	M. L. Barlett *et al.* (Ref. 13)
	(p,p')[b]	800 MeV	2.31	0.029	−0.053	
	(α,α')	50 MeV	2.761	−0.169	−0.154	D. L. Hendrie *et al.* (Ref. 16)
	DDHF	p	2.49	0.057		Negele and Rinker (Ref. 49)
		n	2.46	0.049		

[a]Multipole moments obtained by model independent analysis.
[b]Multipole moments of the imaginary central part of the DOP.

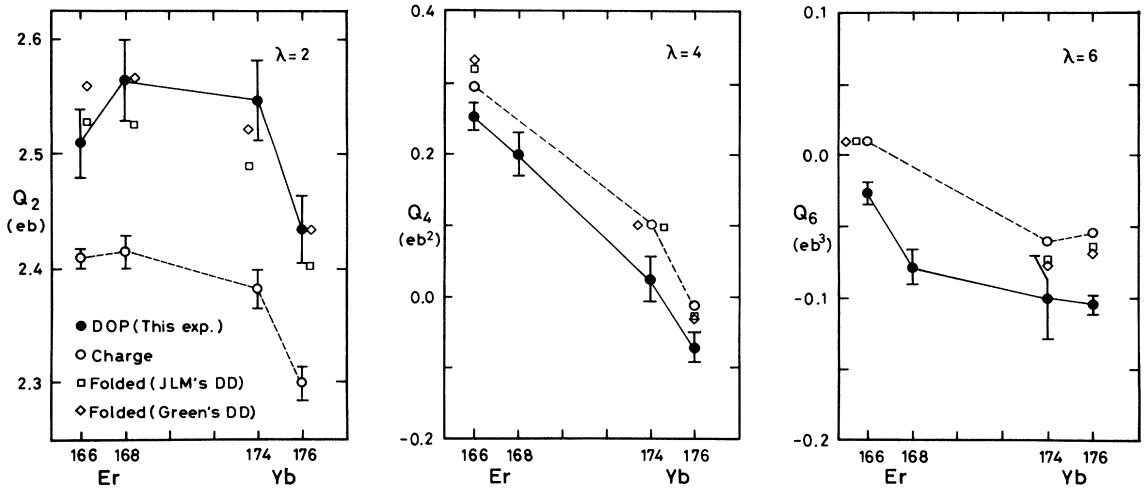

FIG. 8. The closed circles represent the multipole moments of the DOP derived from the present experiment. The open circles represent the charge multipole moments obtained by electron scattering and Coulomb excitation. The open squares represent the multipole moments of the folded potential using JLM's density dependence (DD) and the open diamonds represent those using Green's DD. Some symbols are slightly shifted horizontally to be seen clearly.

density. The DD effective interaction used here reproduces the mean square potential radii as described in Appendix B. In the folding calculation, the point neutron distributions are assumed to be identical to point proton distributions derived from the charge densities.

The multipole moments of the folded potential are listed in Table V and also plotted in Fig. 8. The open squares in Fig. 8 represent the multipole moments using the JLM density dependence and the open diamonds represent Green's density dependence. The quadrupole moments of the folding potential using JLM's DD and Green's DD are about 4.5% and 6.0% larger than those of the charge densities, respectively. The DD effective interaction deepens the potential at the nuclear surface region, and hence the quadrupole moment of the folding potential becomes larger.

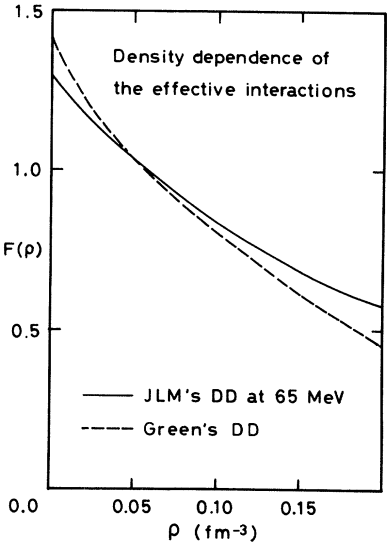

FIG. 9. Density dependence of the effective interaction. The solid line indicates the density dependence based on the JLM model (Ref. 9) at 65 MeV and the dashed line represents the density dependence of Green's model. Both are normalized to unity at one-third of the normal density.

As shown in Fig. 8, the quadrupole moments of the folded potential using the DD effective interaction are in excellent agreement with those of the DOP derived from the coupled channel analysis of the present experiment. Therefore, the main part of the difference in the quadrupole moments between the DOP and charge densities can be explained by the density dependence of the effective interaction.

It was also found that the deviation of the multipole moments of the folded potential from underlying matter distribution depend on the density dependence of the effective interaction dominantly. The finite range M3Y effective interaction and zero range interaction of exchange pseudopotential yield almost equal multipole moments if we use the same density dependence.

Brieva and Georgiev[45] have predicted recently that the multipole moments of the DOP derived from coupled channel calculation will vary with the incident energy. The energy dependence of the multipole moments of the DOP proposed by them is attributed to the fact that the density dependence of the effective interaction varies with the incident energy. It has been also reported by JLM (Ref. 9) that the density dependence of the volume integral of the effective interaction is altered with the incident energy by the BHF calculation. The enhancement of the quadrupole moment of the DOP from underlying matter distribution at 65 MeV in the calculation by Brieva and Georgiev[45] for ^{154}Sm is about 4%, and this is consistent with our data and also with our calculations (4.5—6 %).

D. Higher multipole moments

It is well known[16,46–48] that in the region of rare earth nuclei, the hexadecapole moment has the largest positive value near the Sm isotopes and then decreases gradually as

TABLE V. Results of folding calculations.

Nucleus		Q_2 (e b)	Q_4 (e b^2)	Q_6 (e b^3)	$\langle r^2 \rangle$ (fm^2)
^{166}Er	(p,p′) exp.[a]	2.511 ±0.032	0.252±0.020	−0.025±0.007	35.68
	folded (no DD)[b]	2.410	0.294	0.010	30.01
	folded (JLM's DD)[c]	2.524	0.320	0.010	33.41
	folded (Green's DD)[d]	2.562	0.330	0.009	34.56
^{168}Er	(p,p′) exp.[a]	2.564 ±0.038	0.198±0.031	−0.078 ±0.012	35.79
	folded (no DD)[b]	2.415			30.28
	folded (JLM's DD)[c]	2.526			33.72
	folded (Green's DD)[d]	2.565			34.88
^{174}Yb	(p,p′) exp.[a]	2.547 ±0.039	0.025±0.031	−0.099 ±0.029	36.32
	folded (no DD)[b]	2.384	0.102	−0.060	31.59
	folded (JLM's DD)[c]	2.489	0.101	−0.073	34.94
	folded (Green's DD)[d]	2.523	0.103	−0.077	36.02
^{176}Yb	(p,p′) exp.[a]	2.436±0.032	−0.071±0.020	−0.104 ±0.007	36.17
	folded (no DD)[b]	2.300	−0.013	−0.054	31.67
	folded (JLM's DD)[c]	2.403	−0.026	−0.064	35.01
	folded (Green's DD)[d]	2.437	−0.030	−0.068	36.10

[a]Multipole moments of the DOP derived from the present experiment.
[b]Multipole moments of the folded potential using no density dependence. They are equal to charge multipole moments.
[c]Multipole moments of the folded potential using JLM's DD.
[d]Multipole moments of the folded potential using Green's DD.

the target mass number increases. Our data show the same tendency as shown in Fig. 8. The hexadecapole moment changes its sign between ^{174}Yb and ^{176}Yb.

The excitation to the 4^+ state is caused by the double-step process through the quadrupole moment and by the single-step process through the hexadecapole moment dominantly. The observed difference in the angular distributions of the 4^+ state between Er and Yb isotopes is based on the interference between these two different dominant processes.

As shown in Fig. 8, the trends of the hexadecapole moments of the DOP and the charge densities are similar. However, hexadecapole moments of the DOP are slightly smaller than the charge hexadecapole moment, and this phenomena cannot be explained by the density dependence of the effective interaction on the assumption that the proton and neutron distributions are identical. The DDHF calculation by Negele and Rinker[49] suggests that the hexadecapole moments of the proton and neutron distributions are different. There is also a possibility that these differences may arise from the different treatments of the form factors in the analysis of the electron scattering[33,34] and hadron scattering.

Although the hexacontatetrapole ($\lambda=6$) moments of the DOP and charge densities have similar trends, the hexacontatetrapole moments of the charge densities are about 0.05 mb^3 larger than those of the DOP in all three nuclei. Since the higher order multipole moments are supposed to be sensitive to the nuclear structure, for example, the difference between the proton and neutron distributions due to the difference in the occupations of the nuclear shells, further precise and systematic measurements are necessary for higher multipole moments using both hadronic and electromagnetic probes.

E. Multipole moments in comparison with other proton scattering

The multipole moments obtained by inelastic scattering of 134 MeV polarized protons[14] from ^{166}Er are listed in Table IV. According to the JLM calculation[9] the slope of the density dependence of the effective interaction at 134 MeV which is normalized at one-third of the normal density is similar (although a little steeper) to that at 65 MeV. Therefore the multipole moments of the DOP at 134 and 65 MeV are expected to be almost equal. The multipole moments of the DOP at 134 MeV agree with our results within the error, although the separation between the 0^+ and 2^+ states is not so good in the experiment at 134 MeV. This fact suggests that even in the intermediate energy region, the density dependence of the effective interaction cannot be neglected.

It has been reported[12] that the quadrupole moments of the DOP obtained by 35 MeV unpolarized protons are systematically smaller ($\lesssim 6\%$) than the charge quadrupole moments. This result cannot be explained by the density dependence of the effective interaction. The density dependence of the effective interaction causes the opposite sign in the deviation in the quadrupole moment. It is supposed that the reaction mechanism is not so simple at 35 MeV, or that the simple folding model would break down at that energy.

It is also interesting that the experiment and the analysis of proton inelastic scattering from ^{176}Yb at 800

MeV (Ref. 13) showed the multipole moments of the imaginary central part of the DOP to be almost equal to the charge multipole moments. This can be explained by the fact that the scattering at 800 MeV is caused dominantly by the imaginary part of the optical potential and also that the impulse approximation is applicable fairly well at that energy.

VI. SUMMARY AND CONCLUSION

We have measured the differential cross sections and analyzing powers of elastic and inelastic scattering of 65 MeV polarized protons from ^{166}Er, ^{168}Er, ^{174}Yb, and ^{176}Yb. We have analyzed for the members of the ground state rotational band up to the $J^{\pi}=6^{+}$ state using coupled channel calculations assuming the axially symmetric rotational model. In the coupled channel calculation, the multipole moments of each form factor of the optical potential were set to be equal. Excellent fits have been obtained for both cross sections and analyzing powers for 0^{+}, 2^{+}, and 4^{+} states and fairly good fits for the 6^{+} state.

We have compared the SOP that reproduces only the elastic scattering with the DOP that was derived from the coupled channel calculations and observed similar differences as reported in our previous paper.[2] The volume integrals of real central potentials per nucleon of the DOP are about 14—17 MeV fm^3 larger than those of the SOP. The effect of the collective excitations on the real central potential is repulsive.

The multipole moments of $\lambda=2$, 4, and 6 of the DOP have been compared with those of the charge densities. They are generally in good agreement with the electromagnetic measurement. However, it was found that the quadrupole moments of the DOP are 4—6% larger than those of the charge densities. The folding model calculations show that the quadrupole moments of the folded potential using density dependent effective interaction are about 5% larger than those of the charge densities. Therefore, the main difference in the quadrupole moments between the DOP and charge distributions can be explained by the density dependence of the effective interaction.

The trends of the hexadecapole moments and hexacontatetrapole moments of the DOP and charge densities are similar, but the latter are slightly larger and these phenomena cannot be explained by the density dependence of the effective interaction on the assumption that the proton and neutron distributions are identical. Since the higher multipole moments are thought to sensitively reflect nuclear fine structure, further precise and systematic measurements are necessary using both hadron probes and electrons.

The precise experiment on the deformed nuclei using 65 MeV polarized protons has exhibited that the effective two-body interaction between projectile and target nucleons has density dependence. This reflects the dynamical effect of a nucleus as a many-body system of the nucleons.

ACKNOWLEDGMENTS

The authors wish to express their thanks to Prof. H. Ikegami, Dr. S. Morinobu, Dr. M. Fujiwara, and Dr. Y. Fujita for their advice in the operation of the spectrograph RAIDEN and focal plane counter system, and to Dr. K. Hatanaka for the operation of the polarized ion source. Sincere thanks are also expressed to Prof. M. N. Harakeh from Kernfysisch Versneller Instituut (KVI) for his comments and discussions, and Prof. J. Raynal from Saclay for the usage of the code ECIS79. Most of the coupled channel calculation was done with FACOM M-180-IIAD at RCNP and partially with FACOM M-382 at the Data Processing Center, Kyoto University. This experiment has been performed at the Research Center for Nuclear Physics, Osaka University, under Program No. 15A01 and was supported in part by a Grant-in-Aid for Scientific Research No. 57540141 and No. 57460014 of the Japan Ministry of Education, Science, and Culture.

APPENDIX A: FOLDING CALCULATION USING DENSITY DEPENDENT EFFECTIVE INTERACTION

The folding equation using a density dependent effective interaction is written as

$$U_{\rm opt}(\vec{r})=\int \rho(\vec{r}\,')V_{\rm eff}\left[\,|\,\vec{r}-\vec{r}\,'\,|\,,\rho\left[\frac{\vec{r}+\vec{r}\,'}{2}\right]\right]d\vec{r}\,' , \quad \text{(A1)}$$

where the effective interaction $V_{\rm eff}(r,\rho)$ is a function of both the distance and the density.

The density dependent effective interactions used are written as follows:

$$V_{\rm eff}(r,\rho)=V^{0}(r)F(\rho) , \quad \text{(A2)}$$

$$V^{0}(r)=V_{D}^{0}(r)+V_{\rm ex}^{0}(r) , \quad \text{(A3)}$$

where $V_{D}^{0}(r)$ and $V_{\rm ex}^{0}$ represent the direct and exchange parts of the effective interaction, and $F(\rho)$ represents the density dependence. We used the midway density between two interacting nucleons in the density dependent function. For the direct part of the effective interaction, we used the isoscalar part of the M3Y by Bertsch *et al.*[41] that is parametrized to reproduce the harmonic oscillator matrix elements of Elliott *et al.*[42] for odd states and the effective G-matrix elements of the Reid soft-core potential for even states. For the knock-on exchange, the pseudopotential of the δ function proposed by Satchler and Love[44] was used:

$$V_{D}^{0}(r)=(7999e^{-4r}/4r-2134e^{-2.5r}/2.5r)\ \text{MeV} , \quad \text{(A4)}$$

$$V_{\rm ex}^{0}(r)=-276(1.-0.005E_{\rm p}/A_{\rm p})\delta(r)\ \text{MeV} , \quad \text{(A5)}$$

where $E_{\rm p}$ and $A_{\rm p}$ represent the energy and the mass number of the projectile. This form of the density dependent effective interaction was proposed by Kovos *et al.*[43] in the double folding calculation of the alpha particle optical potential. We used two types of the density dependence function; the first one has the following form:

$$F_{\rm JLM}(\rho)=C(1.0+\alpha e^{-\beta\rho}) , \quad \text{(A6)}$$

where the parameters α, β, and C were chosen to repro-

duce the results of the BHF calculation for nuclear matter by Jeukenne, Lejeune, and Mahaux (JLM).[9] At 65 MeV, $\alpha=7.0$, $\beta=5.0$, and $C=0.159$ were obtained.

The second one has Green's density dependence linear in $\rho^{2/3}$:[4-7]

$$F_G(\rho)=C(1.0-A\rho^{2/3}) . \quad \text{(A7)}$$

In our calculation, the density dependence coefficient A and the normalization factor C were set as $A=2.0$ and $C=1.42$. The value of the normalization factor C does not affect the multipole moments of the folding potential.

The matter distributions were assumed to be deformed Fermi distributions as follows:

$$\rho(r,\theta)=\rho_0\{1.0+\exp[[r-R(\theta)]/a_m]\}^{-1} , \quad \text{(A8)}$$

$$R(\theta)=R_m\left[1.0+\sum_\lambda \beta_\lambda^m Y_{\lambda 0}(\theta)\right] . \quad \text{(A9)}$$

We assumed that the point neutron distributions are identical to the point proton distributions derived from charge densities.[33,34] The matter diffuseness was fixed as $a_m=0.470$.[1] The mean square radius of the point proton distribution and the charge distribution have a following relation,[44]

$$\langle r^2\rangle_p=\langle r^2\rangle_{\text{charge}}-0.76+0.11(N/Z)\ (\text{fm}^2) , \quad \text{(A10)}$$

where $\langle r^2\rangle_p$ represents the mean square radius of point proton distributions. In this equation the correction from the charge distribution in the neutron itself is included. The deformation parameters β_λ^m were calculated so as to reproduce the equal multipole moments to the charge densities. The matter distributions used are listed in Table VI. For ^{168}Er and ^{174}Yb we used the same geometrical parameter (reduced radii and diffuseness) as ^{166}Er and ^{176}Yb.

The folding potentials were calculated in three-dimensional coordinate space, and the results are listed in Table IV. The accuracy of the numerical calculation of the multipole moments of the folding potential was checked using Satchler's theorem in the density independent case.

TABLE VI. Matter distributions.

	^{166}Er[a]	^{168}Er[b]	^{174}Yb[b]	^{176}Yb[a]
R_m	6.090	6.114	6.310	6.334
a_m	0.470	0.470	0.470	0.470
β_2^m	0.3334	0.3394	0.3126	0.3073
β_4^m	0.0171	(−0.0132)	−0.0249	−0.0537
β_6^m	−0.0148	(−0.0382)	−0.0218	−0.0080
Q_2 (e b)	2.41	2.41	2.38	2.30
Q_4 (e b^2)	0.294	(0.15)	0.102	−0.013
Q_6 (e b^3)	0.010	(−0.06)	−0.060	−0.054

[a]These are point proton distributions of deformed Fermi forms derived from the charge densities obtained by the electron scattering data (Ref. 33) assuming that the diffuseness a_m is 0.47 fm.

[b]These geometrical parameters (reduced radius r_m and diffuseness a_m) are equal to those of the isotopes.

APPENDIX B: MEAN SQUARE RADII AND THE RANGE OF THE EFFECTIVE INTERACTION

The mean square radii (MSR) of the potential are given as follows:

$$\langle r^2\rangle_{\text{pot}}=\frac{1}{Jv}\int V_R(r,\theta)r^4 dr\, d\Omega , \quad \text{(B1)}$$

where $V_R(r,\theta)$ represents the real central part of the DOP. The MSR of the matter distribution are given by replacing $V_R(r,\theta)$ with $\rho(r,\theta)$ in Eqs. (B1) and (6).

Table V lists the MSR of charge densities obtained from electron scattering[33,34] and the MSR of the DOP that reproduced our experimental data. Also, the MSR of the folded potentials using the density independent and two kinds of DD effective interactions are listed in the table. As shown in the table, the MSR of the folded potentials using density independent effective interaction (M3Y + δ) are about 15% smaller than those of our DOP. However the MSR of the folded potentials using the DD effective interaction are almost equal to those. This can be explained by the same reason as the quadrupole moment, that the density dependent effective interaction deepens the potential at the nuclear surface and therefore the MSR of the potentials become larger.

Now we define the mean square range of the effective interaction as follows:

$$\langle r^2\rangle_{\text{int}}=\langle r^2\rangle_{\text{pot}}-\langle r^2\rangle_{\text{matt}} . \quad \text{(B2)}$$

The systematic study of the elastic proton scattering at 65 MeV has exhibited that the range of the effective interaction depends on the mass number of the target nuclei.[1] Recently, Srivastava[50] has pointed out the possibility of explaining this mass number dependence in terms of the density dependence of the effective interaction. Therefore, we have calculated the folded potential for ^{16}O, ^{40}Ca, ^{90}Zr, and ^{208}Pb in order to examine this possibility. Since the MSR of the nuclear matter distributions are linear in $A^{2/3}$, where A is a mass number of the target nuclei, we parametrized the range of the effective interaction and the MSR of the potential as $(aA^{2/3}+b)$. According to Srivastava,[50] the range of the DD effective interaction is linear in $A^{1/3}$ under some assumptions. However, the correlation coefficient was found to be almost equal to unity even if we fit it to the form as $(aA^{2/3}+b)$. By the least-square fit, we have obtained the following results.

The ($M3Y+\delta$) effective interactions with JLM's density dependence and Green's density dependence have the following target mass number dependence:

$$\langle r^2\rangle_{\text{int}}=4.44+0.070A^{2/3}\ (\text{fm}^2)\ \text{(JLM's DD)} , \quad \text{(B3)}$$

$$\langle r^2\rangle_{\text{pot}}=6.36+0.888A^{2/3}\ (\text{fm}^2)\ \text{(JLM's DD)} , \quad \text{(B4)}$$

$$\langle r^2\rangle_{\text{int}}=4.69+0.092A^{2/3}\ (\text{fm}^2)\ \text{(Green's DD)} , \quad \text{(B5)}$$

$$\langle r^2\rangle_{\text{pot}}=6.69+0.916A^{2/3}\ (\text{fm}^2)\ \text{(Green's DD)} . \quad \text{(B6)}$$

Our experimental results[1] are as follows:

$$\langle r^2\rangle_{\rm int}=4.24\pm0.24+(0.132\pm0.013)A^{2/3}\ ({\rm fm}^2)\ , \quad \text{(B7)}$$

$$\langle r^2\rangle_{\rm pot}=6.42\pm0.21+(0.937\pm0.012)A^{2/3}\ ({\rm fm}^2)\ . \quad \text{(B8)}$$

The closed circles in Fig. 10 represent the MSR of the real central part of the optical potential. Other data plotted on the figure were taken from Ref. 1. In the deformed region, the MSR of the potential becomes large due to the deformation effect. So we also show the MSR for these nuclei in the open circles where all the deformation parameters are set to zero. The solid line indicates the MSR of the folded potential using the density dependent (M3Y + δ) effective interaction with Green's density dependence. The dashed line indicates those with JLM's density dependence. As shown in the figure, the effective interaction with Green's density dependence reproduces the MSR quite well. The mass number dependence of the range of the effective interaction can be explained by the density dependence of the effective interaction. The dotted line shows the MSR of the folded potential using the pure M3Y effective interaction without the δ function of the pseudopotential. The dash-dotted line represents the MSR using the (M3Y + δ) effective interaction without density dependence. By the presence of the zero-range interaction, the MSR of this interaction is smaller than the experimental results. Although the DD effective interactions employed here are semiphenomenological, it was found that they reproduce the experimental results fairly well.

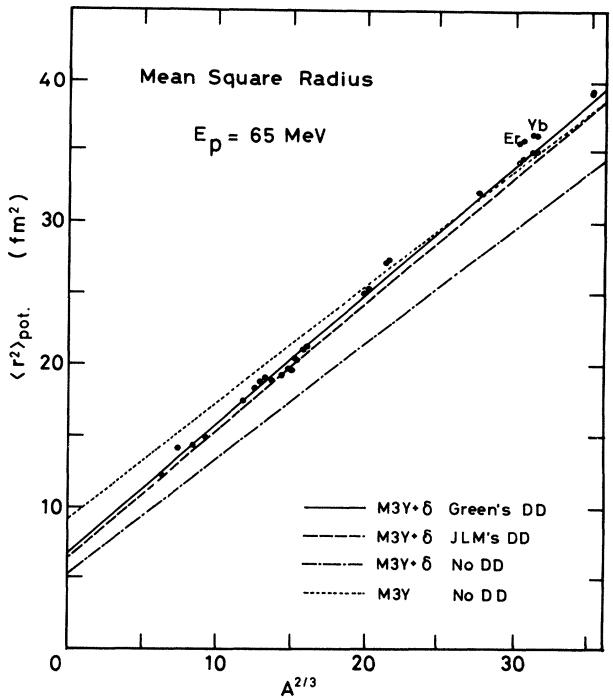

FIG. 10. MSR of the potential. The closed circles represent the MSR of the optical potentials at E_p=65 MeV. The values except for present experiment are taken from Ref. 1. The open circles for deformed nuclei are MSR where all the deformation parameters are set to zero. Four kinds of lines indicate the results of folding calculations.

*Present address: Research Center for Nuclear Physics, Osaka University, Osaka, Japan.
†Present address: Simazu seisakusho, Kyoto 606, Japan.
‡Present address: Institute of Physics, University of Tsukuba, Nishihari-Gun, Ibaragi 305, Japan.

[1]H. Sakaguchi, M. Nakamura, K. Hatanaka, A. Goto, T. Noro, F. Ohtani, H. Sakamoto, H. Ogawa, and S. Kobayashi, Phys. Rev. C 26, 944 (1982).
[2]F. Ohtani, H. Sakaguchi, M. Nakamura, T. Noro, H. Sakamoto, H. Ogawa, T. Ichihara, M. Yosoi, and S. Kobayashi, Phys. Rev. C 28, 120 (1983).
[3]G. R. Satchler, J. Math. Phys. 13, 1118 (1972).
[4]A. M. Green, Phys. Lett. 24B, 384 (1967).
[5]D. K. Srivastava, N. K. Ganguly, and P. E. Hodgson, Phys. Lett. 51B, 439 (1974).
[6]W. D. Meyer, Nucl. Phys. A266, 379 (1976).
[7]F. Petrovich, D. Stanley, and J. J. Bevelacqua, Phys. Lett. 71B, 259 (1977).
[8]F. A. Brieva and J. R. Rook, Nucl. Phys. A291, 299 (1977); A291, 317 (1977).
[9]J.-P. Jeukenne, A. Lejeune, C. Mahaux, Phys. Rev. C 16, 80 (1977).
[10]J. K. Hamilton and R. S. Mackintosh, J. Phys. G 4, 557 (1978).
[11]R. S. Mackintosh, J. Phys. G 4, 547 (1978).
[12]C. H. King, J. E. Finck, G. M. Crawley, J. A. Nolen, Jr., and R. M. Ronningen, Phys. Rev. C 20, 2084 (1979).
[13]M. L. Barlett, J. A. McGill, L. Ray, M. M. Barlett, G. W. Hoffmann, N. M. Hintz, G. S. Kyle, M. A. Franey, and G. Blanpied, Phys. Rev. C 22, 1168 (1980).
[14]R. M. Ronningen, G. M. Crawley, N. Anantaraman, S. M. Banks, B. M. Spicer, G. G. Shute, V. C. Officer, J. M. R. Wastell, D. W. Devins, and D. L. Friesel, Phys. Rev. C 28, 123 (1983).
[15]H. Clement, R. Frick, G. Graw, F. Merz, H. J. Scheerer, P. Schiemenz, N. Seichert, and S. T. Hsun, Phys. Rev. Lett. 48, 1082 (1982).
[16]D. L. Hendrie, N. K. Glendenning, B. G. Harvey, O. N. Jarvis, H. H. Duhm, J. Saudinos, and J. Mahoney, Phys. Lett. 26B, 127 (1968); N. K. Glendenning, D. L. Hendrie, and O. N. Jarvis, *ibid.* 26B, 131 (1968).
[17]K. Hatanaka, N. Matsuoka, T. Saito, K. Hosono, M. Kondo, S. Kato, T. Higo, S. Matsuki, and K. Ogino, Nucl. Phys. A403, 109 (1983).
[18]H. Ikegami, S. Morinobu, I. Katayama, M. Fujiwara, and S. Yamabe, Nucl. Instrum. Methods 175, 335 (1980).
[19]K. Imai, N. Tamura, and K. Nisimura, Research Center for Nuclear Physics Annual Report, 1976, p. 23.
[20]H. Ikegami, I. Katayama, M. Fujiwara, S. Morinobu, Y. Fujita, and H. Ogata, Research Center for Nuclear Physics Annual Report, 1976, p. 76.
[21]T. Ichihara, H. Sakaguchi, K. Hatanaka, M. Fujiwara, and K. Hosono, Research Center for Nuclear Physics Annual Report, 1981, p. 194.

[22]Y. Fujita, K. Nagayama, M. Fujiwara, S. Morinobu, T. Yamazaki, and H. Ikegami, Nucl. Instrum. Methods 196, 249 (1982).
[23]I. Katayama and H. Ogata, Nucl. Instrum. Methods 174, 295 (1980).
[24]J. Raynal, code MAGALI, Saclay (unpublished).
[25]T. Tamura, Rev. Mod. Phys. 31, 679 (1965).
[26]J. Raynal, code ECIS79, Saclay (unpublished).
[27]J. Raynal, International Atomic Energy Agency Report IAEA-5MR-818, 1972, p. 75.
[28]J. Raynal, Phys. Rev. C 23, 2571 (1981).
[29]M. N. Harakeh, Kernfysisch Versneller Instituut Internal Report KVI-77, 1977.
[30]M. N. Harakeh (private communications).
[31]R. S. Mackintosh, Nucl. Phys. A266, 379 (1976).
[32]T. Cooper, W. Bertozzi, J. Heisenberg, S. Kowalski, W. Turchinetz, C. Williamson, L. Cardman, S. Fivozinsky, J. Lightbody, Jr., and S. Penner, Phys. Rev. C 13, 1083 (1976).
[33]C. W. Creswell, Ph.D. thesis, MIT, 1977 (unpublished).
[34]T. Sasanuma, Ph.D. thesis, MIT, 1979 (unpublished).
[35]H. J. Wollersheim, W. Wilcke, and T. W. Elze, Phys. Rev. C 11, 2008 (1975).
[36]J. S. Greenberg and A. H. Shaw, J. Phys. Soc. Jpn. Suppl. 34, 362 (1973).
[37]I. Y. Lee, J. X. Saladin, J. Holden, J. O'Brien, C. Baktash, C. Bemis, Jr., P. H. Stelson, F. K. McGowan, W. T. Milner, J. L. C. Ford, Jr., R. L. Robinson, and W. Tuttle, Phys. Rev. C 12, 1483 (1975).
[38]H. Fisher, D. Kamke, H. J. Kittling, E. Kuhlmann, H. Plicht, and R. Schormann, Phys. Rev. C 15, 921 (1977).
[39]H. J. Wollersheim, W. Wilcke, Th. W. Elze, and D. Pelte, Phys. Lett. 48B, 323 (1974).
[40]K. A. Erb, J. E. Holden, I. Y. Lee, J. X. Saladin, and T. K. Saylor, Phys. Rev. Lett. 29, 1010 (1972).
[41]G. Bertsch, J. Borysowicz, H. McManus, and W. G. Love, Nucl. Phys. A284, 399 (1977).
[42]J. P. Elliott, A. D. Jackson, H. A. Mavromatis, E. A. Sanderson, and B. Singh, Nucl. Phys. A121, 241, (1968).
[43]A. M. Kovos, B. A. Brown, P. E. Hodgson, G. R. Satchler, and A. Budzanowski, Nucl. Phys. A384, 65 (1982).
[44]G. R. Satchler and W. G. Love, Phys. Rep. 55, 183 (1979).
[45]F. A. Brieva and B. Z. Georgiev, Nucl. Phys. A308, 27 (1978).
[46]N. K. Glendenning and R. S. Mackintosh, Phys. Lett. 29B, 629 (1969).
[47]S. G. Nilsson, C. F. Tsang, A. Sobiczewski, Z. Szymanski, S. Wycech, C. Gustafson, I. L. Lamm, P. Moller, and B. Nillson, Nucl. Phys. A131, 1 (1969).
[48]G. F. Bertsch, Phys. Lett. 26B, 130 (1968).
[49]J. W. Negele and G. Rinker, Phys. Rev. C 15, 1499 (1977).
[50]D. K. Srivastava, Phys. Lett. 113B, 353 (1982).